Study of Electrochemical Impedance of a Continuous Glucose Monitoring Sensor and its Correlation with Sensor Performance

Sara S. Ghoreishizadeh*†, Xiaotian Zhang†, Sanjiv Sharma‡, Pantelis Georgiou†
†Dept. of Electrical & Electronic Eng., Centre for Bio-Inspired Technology, Imperial College London, UK
‡ College of Engineering, Swansea University, UK, * Email: s.ghoreishizadeh14@imperial.ac.uk

***Abstract*—In this work, we study the change in the sensitivity and the electrochemical impedance of continuous glucose monitoring sensors over time. 28-day sensitivity and EIS measurement results on four similar sensors are presented. The sensitivity of the sensor is observed to be related to its double-layer capacitance and charge-transfer resistance, based on results acquired from a sensor that showed substantial sensitivity drop. Two data clusters are extracted that relate the sensor sensitivity to its impedance before and after the sensitivity drops by more than 50%.**

I. Introduction

The next generation of medical devices are emerging to enable continuous health-care monitoring of patients at home [1], [2]. Such devices use electrochemical sensors to measure metabolites in a fast, inexpensive and reliable way. A notable example that is commercially available is continuous glucose measurement (CGM) device that uses enzymatic electrochemical glucose sensor for management of diabetes [3].

One of the major challenges in electrochemical sensors is their constant need for calibration and limited life-time. This is partly due to the biofouling that occurs during the implanation period. The calibration is in particular crucial as the sensitivity of the sensor changes over time even during its lifetime. For example, a calibration step for the CGM sensor is traditionally done through a finger-stick test, and is required at least once a day to obtain accurate and reliable results [4]. This takes extra time and causes inconvenience for diabetic subjects. As a result, it is necessary to investigate methods to simplify conventional calibration process towards lower cost, more convenient, and less time-consuming options.

The electrochemical sensor can be modeled by a network of capacitors and resistors representing its electrical impedance. The electrical impedance of the glucose sensors has been studied in the literature where in particular one impedance parameter (i.e. the charge transfer resistance) is shown to be dependant on the glucose concentration [5], [6] and on the sensor fabrication steps [7].

We hypothesized that some parameters in the sensor impedance have strong correlation with the sensor performance. This has been experimentally proven for the amperometric gas sensors, where the double layer capacitance of the sensor is shown to be linearly proportional to the sensitivity of the sensor [8]. The impedance spectroscopy has been also used to determine the health of the Lithium-ion battery cells [9], electric double-layer ultracapacitors [10], fuel cell systems [11] and glucose sensors [12] among other applications [13]. Motivated by these promising results, in this work we make an attempt to find the correlation between the sensitivity of electrochemical biosensors with their impedance.

In this work, we take the commercially available CGM sensor as an example (of electrochemical biosensors) and monitor its impedance and sensitivity over time and study the correlation between them. The discovery of a correlation paves the way to building a self-calibration algorithm. Such an algorithm enables the prediction of sensor performance, in particular its sensitivity, through measuring its impedance.

In the following Section an introduction is given on the electrochemical sensors along with the most common RC-equivalent circuit model. Section III describes the material and methods. Section IV demonstrates the measurement result and discussion followed by the conclusions and future work.

II. Electrochemical Sensors

The electrochemical glucose sensor is a three-electrode-based electrochemical cell. The electrodes are named working, reference and counter electrodes and their voltage and currents are controlled and measured through a potentiostat. The sensor is made sensitive and selective to glucose through the use of a selective enzyme. Suitable membranes are also designed to cover the sensor to inhibit interferer biomolecules from reaching the sensor [14]. The sensor transforms the chemical quantity (i.e. glucose concentration) into an electrical current which is subsequently measured through a readout circuit. The sensor sensitivity, S, is defined as the ratio of the change in sensor current, I_S, to the change in glucose concentration, C_G:

$$S = \frac{\Delta I_S}{\Delta C_G} \tag{1}$$

A. RC-Model of Electrochemical Sensors

The structure of the electrochemical cell can be interpreted by its impedance measured under the excitation of a sinusoidal signal with relatively small amplitude. The cell can be modeled on the basis of its impedance using an equivalent circuit that creates a current with an identical amplitude and phase characters to the real cell, once excited with the same ac voltage [15]. Among the existing models, Randles equivalent

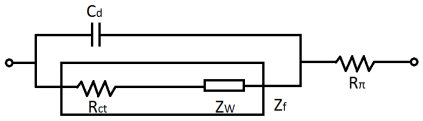

Fig. 1. The typical Randles equivalent model for an electrochemical cell.

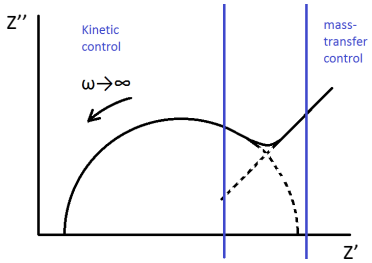

Fig. 2. Nyquist plot of the Randles Model showing a semi-circle at high frequencies and a unity slope line at low frequencies

circuit [16] is the most frequently used one which is also adopted in this work to model the sensor.

The schematic of the model is shown in Fig. 1 where R_π, represents the resistance of the solution (mainly electrolyte). The interface of electrode and electrolyte is modelled by C_d the double-layer capacitance [17] in parallel with the faradaic impedance, Z_f. The parallel structure was introduced to reflect that the total sensor current, I_S, consists the double-layer charging current, I_c, and the faradaic process, I_f:

$$I_S = I_c + I_f \tag{2}$$

The general faradaic impedance Z_f consists of R_{ct}, the charge-transfer resistance, which is mainly due to oxygen reduction reaction, in series with the *Warburg* impedance, Z_w, which represents the resistance to mass transfer process [15]. Assuming a semi-infinite linear diffusion, the Z_w can be represented by two frequency-dependent real and imaginary elements R_w and C_w [18]:

$$Z_w = R_w + \frac{1}{j\omega \cdot C_w} \tag{3}$$

$$R_w = \sigma\omega^{-1/2} \tag{4}$$

$$Z_{C_w} = -j/(\omega C_w) = -j\sigma\omega^{-1/2} \tag{5}$$

Where σ is the Warburg diffusion coefficient of ions in the electrolyte and has the unit of $\Omega \cdot s^{-1/2}$. The Randles model is a simplified model which considers the interface of electrode and electrolyte as a pure capacitor C_d. This element in reality, named constant phase element (CPE) and is frequency dependent. The constant phase phenomenon occurs at the interface of metal, insulator and solution [15].

B. Mass and Kinetic regions

Since faradaic impedance is frequency-dependent, EIS measurement are usually conducted at a wide range of frequencies [19]. By studying the Bode and Nyquist plots of the Randles equivalent circuit, theoretical deductions at both extreme frequency ends can be made for simplicity. At low frequencies the imaginary part of the impedance can be simplified to [15]:

$$Z'' = Z' - R_\pi - R_{ct} + 2\sigma^2 C_d \tag{6}$$

here, Z'' is a linear function of Z' with a unity slope as depicted in Fig. 2. The interception point with the x-axis is at $Z' = R_\pi - R_{ct} + 2\sigma^2 C_d$.

Equation 6 indicates that only the *Warburg* impedance affects the shape of spectroscopy plot at low frequencies, and the linearity of the Nyquist plot in this region is considered as a behavior of a process mainly controlled by diffusion of ions to and from the electrode. This is commonly referred to as the mass-transfer operation region [15].

At high frequencies the Warburg element becomes insignificant. Thus the relationship between the real and imaginary parts of the impedance can be written as:

$$\left(Z' - R_{pi} - \frac{R_{ct}}{2}\right)^2 + Z''^2 = \left(\frac{R_{ct}}{2}\right)^2 \tag{7}$$

Here, the Nyquist plot shows a semi-circle behaviour and the region is referred to as the sensor kinetic region. The semi-circle is centered at the point $Z' = R_\pi + \frac{R_{ct}}{2}$ and has a radius of $\frac{R_{ct}}{2}$. By combining these two cases, impedance change in the entire frequency range is illustrated in Figure 2. Further details could be found in [15].

III. Material and Methods

A. Sensors and chemicals

The measurements in this work are focused on the performance of the commercially available Enlite™ (Medtronic Ltd) Glucose Sensor for continuous glucose monitoring in skin interstitial fluid (ISF). The Enlite sensor has three electrodes on a needle-shape flexible substrate with an approximate dimension of 8 mm× 0.3 mm. Four sensors were measured. When not in use, the sensors were stored in a solution containing glucose and albumin with concentration of 5 mM and $30mg/ml$, respectively, to simulate the conditions of ISF [20], [21]. The storage temperature was kept fixed at $37°C$ using a temperature and humidity chamber (model SH221, ESPEC). The $100mM$ PBS solution and $100mM$ dextrose stock solution were made by dissolving the tablets and powder (Sigma Aldrich)in distilled water, respectively.

B. Measurement instrument and techniques

All measurements were performed using an Electrochemical Workstation (CHI760E, CH Instruments, Inc). To find the sensitivity of the sensor, chronoamperometry measurements were performed (at 0.53 V voltage) at multiple concentrations of glucose in Phosphate Buffered Solution (PBS) in the following way. After an initial sensor conditioning (approximately 10 minutes) in PBS, the glucose concentration was increased in 2.5 mM steps to cover the concentration range of 0 to 20 mM. The measurements were repeated everyday for 28 days. EIS measurements (at 5 mV ac voltage superimposed on 0.53 V DC, ranging from 10 Hz to 1 MHz) were also conducted at each concentrations after routine chronoamperometry.

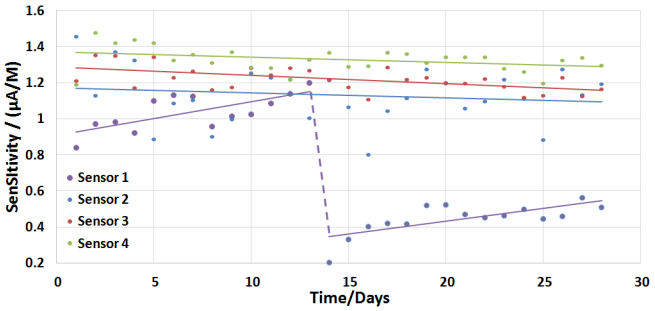

Fig. 3. Measured sensitivity of sensors No. 1, 2, 3, and 4 over time.

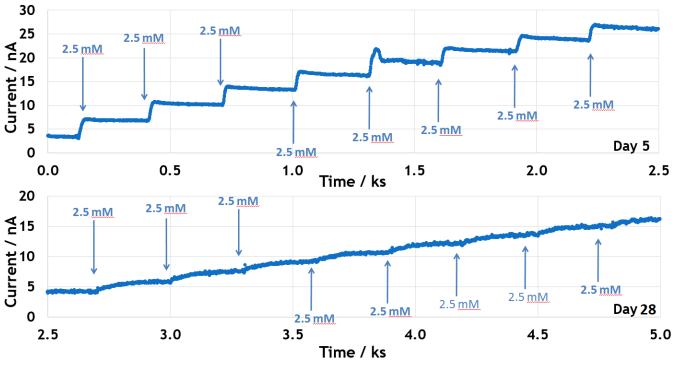

Fig. 4. The chronoamperometry measured on sensor No.1 on day 5 and 28.

C. Data Extraction

Five parameters of the Randles model are extracted from the EIS measurements: R_π, R_{ct}, C_d, and the resistive / capacitive components of the *Warburg* impedance. The parameters are extracted using the circle fitting (Taubin method [22]) and least-squares linear-regression techniques in Matlab. The sensor sensitivity is derived from the calibration line.

IV. Results and Discussion

The measured sensitivity of the sensors versus day from the start of the measurements are plotted in Fig. 3 where a substantial drop to below 50% of the initial sensitivity is observed in sensor No.1 at the 14th day. All the other sensors only show a gradual decrease in sensitivity.

Fig. 4 shows chronoamperometry measurements with sensor No.1 at two days (5th and 28th) before and after the sensitivity drops. Here, an increase in the settling time (i.e. slower response) is observed in addition to the reduced current-step size at day 28th compared to day 5th.

The measured Nyquist plots (see Fig. 5) show a change in the kinetic region of Sensor No.1 after day 14th when the sensitivity drops. At a fixed concentration (i.e. 20 mM) the radius of the semi-circle has decreased after day 14th. The extracted charge resistance ,R_{ct}, and double layer capacitance, C_d of sensor No.1 (at 20 mM glucose concentration) are plotted versus the sensor sensitivity in Fig. 6 where each dot indicates one day of measurement. Here two clusters are recognized which imply the existence of a correlation between the sensitivity and C_d: when C_d is about 4 nF, the sensitivity is close to 1.05 nA/mM; When C_d increases to 6.8 nF, the sensitivity has dropped to approximately 0.4 nA/mM. The two clusters are observed to have different R_{ct} values: 1120 and

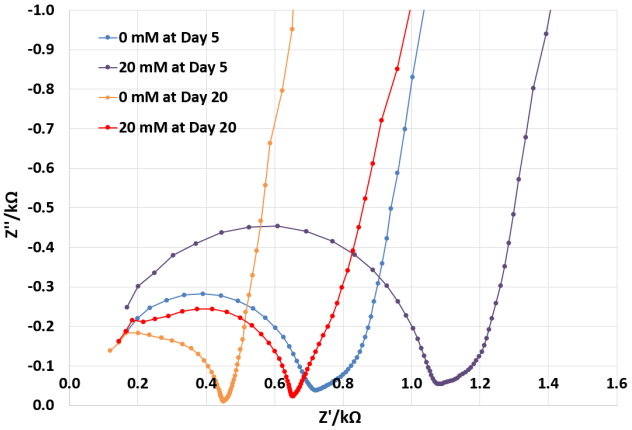

Fig. 5. The Nyquist plot measured on Sensor No.1 on the 5th and 28th days and at two glucose concentrations: 0 mM and 20 mM.

650 Ω. A summary of all the ranges of data points within the two clusters are reported in Table I. The real part of the impedance of sensor No. 1 is plotted versus frequency in Fig. 7 showing a clear change of amplitude in the middle frequencies (eg. at 1 kHz) before and after the sensitivity drop. Although any of R_{ct}, C_d , or $Z'|_{1kHz}$ indicate a change in sensitivity, only the clusters based on C_d are inclusive of all data points.

The acquired data from sensor No. 2,3,4 (at 12.5 mM glucose concentration) fall within a first cluster as no substantial drop in their sensitivity was observed over the 28-day period. The C_d, R_{ct} and $Z'|_{1kHz}$ in the first cluster of all four sensors are within 18% of 4 nF, 30% of 1 kΩ, and 25% of 1.1 kΩ.

The gradual drop in the sensitivity of the sensors could be attributed to the reduced sensitivity of the enzyme over time as well as the biofouling effect where the Albumin protein gradually encloses the sensor. The sudden drop in the sensitivity of sensor no. 1 might be due to the delamination of a biosensing surface in the molecular recognition element layer of the sensor (i.e. the Glucose oxidase enzyme and membranes). The presented results indicate that such a substantial drop in sensor sensitivity can be predicted through the measurement of impedance parameters in parallel with normal chronoamperometry measurement. For example a substantial increase in C_d or decrease in R_{ct} or Z' can be used as an indication of the end of the life-time of the CGM sensor.

The presented results pave the way to developing techniques for sensor self-calibration with impedance spectroscopy. Such a technique can be easily implemented on low-cost technologies such as VLSI design. This enables autonomous devices to be made for continuous metabolite detection. In fact, state-of-the-art already includes low-power compact integrated circuits for impedance spectroscopy [23]–[25]. Ongoing work includes long-time experiments to fully quantify the correlation of sensitivity (both sudden and gradual changes) and C_d in custom-designed electrochemical sensors [26], [27].

V. Conclusion

We studied the electrochemical impedance and the sensitivity of commercially available CGM sensors over a period of 28 days. The results show two data clusters around the initial and the reduced sensitivities of the sensor indicating that

TABLE I
CLUSTERS RELATING SENSITIVITY TO EIS PARAMETERS (DATA OF DAY 14TH IS EXCLUDED FROM R_{ct} AND Z' CLUSTERS)

Sensor No.	cluster 1 C_d (nF)	cluster 1 R_{ct} (Ω)	cluster 1 Z'$_{1kHz}$(kΩ)	S (nA/mM)	cluster 2 C_d (nF)	cluster 2 R_{ct} (Ω)	cluster 2 Z'$_{1kHz}$(kΩ)	S (nA/mM)
1	4±0.3	1120±200	1.2± 0.14	1.05±0.15	6.8±0.6	650±50	0.7±0.04	0.4±0.2
2	3.94±0.29	1060±120	1.18±0.11	1.1±0.3			–	
3	4.2±0.3	914± 144	1.03±0.17	1.2±0.15			–	
4	4.04±0.7	930±250	1.04±0.23	1.32±0.15			–	

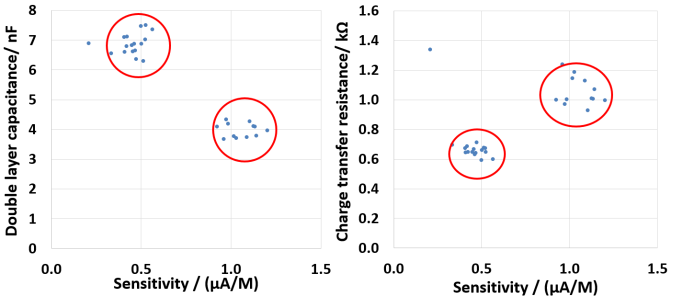

Fig. 6. Measured Sensitivity, S, vs. double layer capacitance, C_d (left) and Charge transfer resistance, R_{ct} (right). All data points are from Sensor No.1.

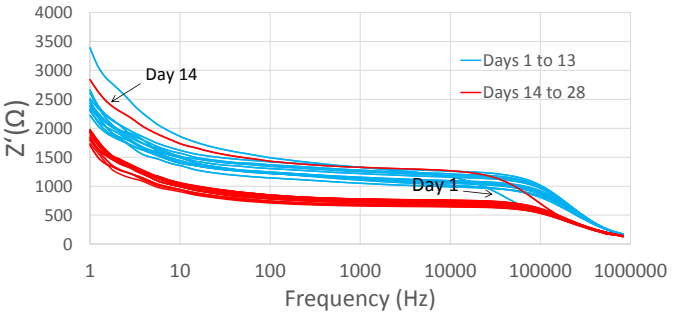

Fig. 7. The real part of impedance vs. frequency for Sensor No.1.

sensitivity is correlated with C_d and R_{ct} as well as $Z'|_{\sim 1kHz}$. A substantial change in any of theses can be used as an indication of the end of the life-time of the CGM sensor. The presented results pave the way to developing techniques for sensor self-calibration with impedance spectroscopy.

VI. ACKNOWLEDGEMENT

The authors would like to thank Prof. Tony Cass for helpful discussions. This work was supported by the Imperial College London Junior Research fellowship Scheme.

REFERENCES

[1] S. Ghoreishizadeh *et al.*, "Sub-mw reconfigurable interface IC for electrochemical sensing," in *IEEE BioCAS 2014 Proceedings*, pp. 232–235.

[2] C. Baj-Rossi *et al.*, "Full fabrication and packaging of an implantable multi-panel device for monitoring of metabolites in small animals," *IEEE Transactions on Biomedical Circuits and Systems (TBCAS)*, vol. 8, no. 5, pp. 636–647, 2014.

[3] A. Facchinetti, "Continuous glucose monitoring sensors: Past, present and future algorithmic challenges," *Sensors*, vol. 16, no. 12, 2016.

[4] Medtronic. Calibrating your sensor. [Online]. Available: https://www.medtronicdiabetes.com/customer-support/sensors-and-transmitters-support/calibration-sensor

[5] H. Wang *et al.*, "A bis-boronic acid modified electrode for the sensitive and selective determination of glucose concentrations," *Analyst*, no. 138, pp. 7146 – 7151, 2013.

[6] R. Karimi *et al.*, "A novel method for glucose determination based on electrochemical impedance spectroscopy using glucose oxidase self-assembled biosensor," *Bioelectrochemistry*, vol. 69, no. 2, pp. 201 – 208, 2006.

[7] C. Hu *et al.*, "Enzyme-labeled Pt@BSA nanocomposite as a facile electrochemical biosensing interface for sensitive glucose determination," vol. 6, 02 2014.

[8] L. Makadmini and M. Horn, "Self-calibrating electrochemical gas sensor," *International Conference on Solid State Sensors and Actuators*, pp. 299–302, 1997.

[9] D. I. Stroe *et al.*, "Diagnosis of lithium-ion batteries state-of-health based on electrochemical impedance spectroscopy technique," in *2014 IEEE Energy Conversion Congress and Exposition (ECCE)*, Sept 2014, pp. 4576–4582.

[10] M. Marracci *et al.*, "Ultracapacitor degradation state diagnosis via electrochemical impedance spectroscopy," *IEEE Transactions on Instrumentation and Measurement*, vol. 64, no. 7, pp. 1916–1921, 2015.

[11] C. de Beer, P. S. Barendse, and P. Pillay, "Fuel cell condition monitoring using optimized broadband impedance spectroscopy," *IEEE Transactions on Industrial Electronics*, vol. 62, no. 8, pp. 5306–5316, Aug 2015.

[12] N. Yang *et al.*, "Application of electrochemical impedance spectroscopy in sensor, systems, devices, and related methods," *Google Patents*.

[13] M. Grossi and B. Ricco, "Electrical impedance spectroscopy (EIS) for biological analysis and food characterization: a review," *Journal of Sensors and Sensor Systems*, vol. 6, no. 2, pp. 303–325, 2017.

[14] C. Baj-Rossi *et al.*, "An innovative system of membranes for the monitoring of endogenous and exogenous metabolites," *BioNanoScience*, vol. 6, no. 2, pp. 85–92, 2016.

[15] A. Bard and L. Faulkner, Eds., *Electrochemical Methods, Fundamentals and Applications*. John Wiley and sons inc., 2001.

[16] J. E. B. Randles, "Kinetics of rapid electrode reactions," *Discussions of the Faraday Society*, vol. 1, no. 11, 1947.

[17] N. Fouquet, "Real time model-based monitoring of a PEM fuel cell flooding and drying out," *Vehicle Power and Propulsion Conference (VPPC), IEEE*, pp. 1–8, 2010.

[18] B. E. Conway, Ed., *Electrochemical Supercapacitors- Scientific Fundamentals and Technological Applications*. Plenum Press, 1999.

[19] E. Barsoukov and J. R. Macdonald, Eds., *Impedance Spectroscopy: Theory, Experiment, and Applications*. Wiley, 2005.

[20] R. Trouillon *et al.*, "Comparative study of the effect of various electrode membranes on biofouling and electrochemical measurements," *Electrochemistry Communications*, vol. 11, no. 7, pp. 1409 – 1413, 2009.

[21] T. Rawson *et al.*, "Towards a minimally invasive device for beta-lactam monitoring in humans," vol. 82, 07 2017.

[22] G. Taubin, "Estimation of planar curves, surfaces and nonplanar space curves defined by implicit equations, with applications to edge and range image segmentation," *IEEE Trans. Pattern Analysis Machine Intelligence*, vol. 13, pp. 1115–1138, 1991.

[23] P. Kassanos, L. Constantinou, I. F. Triantis, and A. Demosthenous, "An integrated analog readout for multi-frequency bioimpedance measurements," *IEEE Sensors Journal*, vol. 14, no. 8, pp. 2792–2800, Aug 2014.

[24] H. Jafari *et al.*, "16-channel CMOS impedance spectroscopy dna analyzer with dual-slope multiplying adcs," *IEEE TBCAS*, vol. 6, no. 5, pp. 468–478, 2012.

[25] M. Bakhshiani *et al.*, "A broadband sensor interface IC for miniaturized dielectric spectroscopy from MHz to GHz," *IEEE Journal of Solid-State Circuits*, vol. 49, no. 8, pp. 1669–1681, Aug 2014.

[26] S. S. Ghoreishizadeh *et al.*, "A differential electrochemical readout ASIC with heterogeneous integration of bio-nano sensors for amperometric sensing," *IEEE TBCAS*, pp. 1–12, 2017.

[27] A. E. Cass and S. Sharma, "Microneedle enzyme sensor arrays for continuous in vivo monitoring," *Methods in Enzymology*, vol. 589, pp. 413 – 427, 2017.